

1 **Self-assembly programming of DNA polyominoes.**

2

3 **Hui San Ong<sup>1</sup>, Mohd Syafiq-Rahim<sup>2</sup>, Noor Hayaty Abu Kasim<sup>3</sup>, Mohd Firdaus-Raih<sup>2</sup>, and**  
4 **Effirul Ikhwan Ramlan<sup>1,4,\*</sup>**

5

6 <sup>1</sup> Natural Computing Laboratory, Department of Artificial Intelligence, Faculty of Computer  
7 Science and Information Technology, University of Malaya, 50603, Kuala Lumpur, Malaysia

8 <sup>2</sup> School of Biosciences and Biotechnology, Faculty of Science and Technology and Institute of  
9 Systems Biology, Universiti Kebangsaan Malaysia, 43600, Bangi, Malaysia

10 <sup>3</sup> Department of Restorative Dentistry, Faculty of Dentistry, University of Malaya, Kuala Lumpur,  
11 Malaysia

12 <sup>4</sup> Centre of Research for Computational Sciences and Informatics for Biology, Bioindustry,  
13 Environment, Agriculture, and Healthcare (CRYSTAL), University of Malaya, 50603 Kuala  
14 Lumpur, Malaysia

15

16 \* effirul@um.edu.my

17

18 **ABSTRACT**

19 **Fabrication of functional DNA nanostructures operating at a cellular level has been accomplished**

20 **through molecular programming techniques such as DNA origami and single-stranded tiles (SST).**

21 During implementation, restrictive and constraint dependent designs are enforced to ensure conformity

22 is attainable. We propose a concept of DNA polyominoes that promotes flexibility in molecular

23 programming. The fabrication of complex structures is achieved through self-assembly of distinct

24 heterogeneous shapes (i.e., self-organised optimisation among competing DNA basic shapes) with total

25 flexibility during the design and assembly phases. In this study, the plausibility of the approach is

26 validated using the formation of multiple 3 x 4 DNA network fabricated from five basic DNA shapes

27 with distinct configurations (monomino, tromino and tetrominoes). Computational tools to aid the

28 design of compatible DNA shapes and the structure assembly assessment are presented. The

29 formations of the desired structures were validated using Atomic Force Microscopy (AFM) imagery.

30 Five 3 x 4 DNA networks were successfully constructed using combinatorics of these five distinct

31 DNA heterogeneous shapes. Our findings revealed that the construction of DNA supra-structures could

32 be achieved using a more natural-like orchestration as compared to the rigid and restrictive

33 conventional approaches adopted previously.

34 Keywords: DNA polyominoes, molecular programming, self-assembly, DNA nanotechnology, DNA  
35 nanofabrication

36

## 37 **1. Introduction**

38 Self-assembly allows DNA molecules to naturally fuse together and form supra-structures (Mao et  
39 al., 2000; Seeman, 1982; Winfree, 1998). The spontaneous reaction via Watson-Crick base pairing  
40 allows the formation of discrete structures with high precision and efficiency. Common approaches in  
41 constructing DNA supra structures include DNA origami (Han et al., 2011; Kuzuya and Komiyama,  
42 2010; Marchi et al., 2014; Rothmund, 2006), molecular tiles (Winfree, 1996), parallelograms from  
43 Holliday junctions (Mao et al., 1999) and single stranded modular motif (Wei et al., 2012; Yin et al.,  
44 2008). These conventional approaches have their limitations (Ke et al., 2012; Ong et al., 2015;  
45 Pinheiro et al., 2011; Wei et al., 2012; Yin et al., 2008). Crucially, the intricate and meticulous  
46 sequence design phase in which the nanostructures were fabricated by generating a definitive set of  
47 DNA sequences. This study attempts to address this issue by allowing the structures to be constructed  
48 autonomously using distinct interchangeable components.

49

50 This is achieved through the formation of desired conformations from a combination of distinct  
51 heterogeneous shapes. This increases the flexibility of constructing DNA nanostructures since the  
52 formation of the structures is achieved through the self-organisation of the competing DNA shapes  
53 without pre-fixed configuration. The core principle is to allow the most preferred shape and sequence  
54 combinations to take precedence (i.e., survival of the fittest). For instance, if  $n$  sets (where  $n$  is more  
55 than 1) of DNAs are initially designed to assemble into the desired conformations, in cases where a  
56 single set of the structure collapsed, the remaining  $n - 1$  sets would be capable to form the target  
57 structure. In fact, individual units inside the  $n - 1$  sets can replace the incompatible unit of the original  
58 set. This interchangeability is a key aspect of the approach. Every component in each set is modular,

59 whereby the failure of any particular unit would not affect the completeness of the set. The mechanism  
60 allows a specific substitution (i.e., to replace any incompatible shapes) or the replacement of the entire  
61 shape configurations to be executed. Therefore, total programmability (i.e., pre-fixed configuration of  
62 binding between shapes) is not promoted in this approach, the formation of the structures is dependent  
63 entirely on the self-organised characteristics of the molecule. This eliminates dependency on successful  
64 wet lab implementation of a particular set. The mechanism employed promotes molecular orchestration  
65 (Zauner, 2005), and in this instance, a mixture of multiple potential sets that self-organised themselves  
66 into the desired configurations (i.e., many to one relationship, where extraction of successful  
67 configurations could be made regardless of the sets).

68

69 The construction of DNA nanostructures (Amir et al., 2014; Benenson et al., 2004; Ding and  
70 Seeman, 2006; Douglas et al., 2012) begins with the sequence design steps. Various strategies such as  
71 strain minimization, sequence symmetry minimization and free energy minimization are employed by  
72 programs such as SEQUIN (Seeman, 1982), Tiamat (Williams et al., 2008), Uniquimer-3D (Zhu et al.,  
73 2009) and GIDEON (Birac et al., 2006) to aid in the sequence generation. In fact, the design of 3D  
74 DNA origami structures is now supplemented by software packages such as caDNAno (Douglas et al.,  
75 2009) that incorporate a graphical user interface. Recently, a program called Polygen has been  
76 developed to aid in the construction of complex atomistic covalently linked DNA nano-cages (Alves et  
77 al., 2016).

78

79 In this study, a computational tool leveraging on the aforementioned strategies such as sequence  
80 symmetry, is extended towards optimising and designing a set of less stringent sequences. Our model  
81 encourages the competition between DNAs to occur in an effort to promote sequence to structure  
82 flexibility. A tool is then created to provide mapping for the competitive shapes by delineating all  
83 probable paths taken by the DNA to form the structures using graph theory (Biggs et al., 1986). This is  
84 essential since molecular self-assembly is asynchronous with a multitude of errors (Rothemund et al.,

85 2004), and probable shapes (i.e., the "best" unit) must compete with the partially probable shapes (i.e.,  
86 the "next best" unit) during the assembly process at all time. The mapping of the paths strategy exerted  
87 in this work could therefore provide insights into the fundamental basis of the structure construction  
88 for the end user.

89

90

## 91 **2. Material and methods**

### 92 **2.1 Fundamental Concepts in DNA polyominoes**

93 This section begins by presenting the fundamental concept in the proposed schema, DNA  
94 polyominoes. Polyominoes shapes (monomino, tromino and tetrominoes) were used as the  
95 representative in demonstrating the feasibility of using multiple elementary blocks in structural  
96 assembly. The hierarchical schema in DNA polyominoes starts with an elementary block, followed by  
97 shapes and then larger structural formations. As a basis, each block used two single-stranded DNAs to  
98 form a block. Then, multiple units of these blocks assembled into a shape. Different shapes would then  
99 assemble into a larger structure (Fig. 1).

100

101 Each of these shapes can comprise of one or more connector on the horizontal sides of the  
102 shape. Its function is to enable the shape to bind to another shape that had a matching connector and  
103 thus forming larger structures. In the context of DNA sequences, the matching connector was defined  
104 as DNA with complementary sticky ends. In total, eight distinct shapes were used and labelled with  
105 specific alphabets. All DNA shapes (Fig. 2) are comprised of four single stranded DNAs except for  
106 shape I (made from two single stranded DNAs).

107

108

109

110

## 111 2.2 DNA segmentation

112 A computational protocol was developed to map the interaction (intermolecular binding) between  
113 DNA nucleotides based on the principle of binding dependencies (Ramlan and Zauner, 2013) between  
114 nucleotides. We implemented an undirected graph representation, in which DNA segments are stored  
115 as nodes that are connected using edges. This allows the automated system to compute all probable  
116 paths taken by each DNA segment (node) in forming the structures. The protocol required each DNA  
117 strand to be separated into different segments based on perfect complementarity (i.e., where all the  
118 intended bases hybridize as specified in the design) between its pairs (Fig. 3).

119

## 120 2.3 Construction of the free energy and binding affinity matrices

121 In order to construct the energy matrix, each segment is represented as node, or vertex.  
122 Thermodynamics free energy between each node were calculated using the program DuplexFold  
123 (Reuter and Mathews, 2010). Default parameters (for the program) were used with the "DNA"  
124 parameter setting. The free energy profile with  $n$  number of nodes resulted in a matrix with  $n$  number  
125 of rows and columns as follows:

$$\begin{bmatrix} X_{1,1} & \dots & X_{1,n} \\ \vdots & \dots & \vdots \\ X_{n,1} & \dots & X_{n,n} \end{bmatrix}$$

126  $X_{i,j} = \Delta G_{i,j}; i, j = 1, 2 \dots n; n = \text{Total number of nodes}$

127 The energy matrix is converted into a binding affinity matrix. The free energy at each position  $\Delta G_{i,j}$   
128 will then be divided by the lowest energy in each row ( $\min(\Delta G_{i,j_{1..n}})$ ), resulting into the probable  
129 binding affinity value between every node. The value of 1.0 indicates the lowest free energy (strongest  
130 binding) between all available bindings. For instance, when the binding affinity between node 1 and  
131 node 2 is 1.0, it indicates that the binding strength of node 1 with node 2 is the strongest compared to  
132 other available binding with the remaining nodes (e.g. 3, 4, 5...etc). The formula for binding affinity is  
133 as follows:

134 Binding affinity for  $P_{i,j} = \frac{\Delta G_{i,j}}{\min(\Delta G_{i,j,1..n})}$

135 Edges connecting nodes with 1.0 binding affinity values represent the most favourable binding  
136 among the  $n$  number of nodes. However, in circumstances where no edges carry the most favourable  
137 binding affinity values (1.0), the highest value will take precedence (in our implementation binding  
138 affinity must be above the threshold value of 0.7).

139

## 140 **2.4 Binding affinity graph: computing the probable paths**

### 141 **2.4.1 Determining the start point**

142 In order to determine the start point, the melting temperature ( $T_m$ ) for every DNA pair  $X_{i,j}$  was  
143 calculated using UNAFold-3.8 (Markham and Zuker, 2008). The DNA pairs with  $T_m$  value equal or  
144 higher than quartile 3 were selected as the start point. For each pair, the strongest node (with lowest  
145 free energy) were selected as the start point and the remaining of the nodes (within the pair) would act  
146 as the sticky ends. These sticky ends would then operate as precursors in determining the node to be  
147 selected next (Supplementary Fig. S1).

148

### 149 **2.4.2 Greedy search phase**

150 The graph would only proceed to the node with the binding affinity value of  $P_{i,j} > 0.7$ . The default  
151 value is fixed at 0.7 to ensure that the graph is restricted to favour only strong estimation values (i.e.,  
152 representative of the preferable binding interactions). Lower assignment of threshold generates  
153 convoluted paths full of weak interactions, which only complicates the search process. For every new  
154 node, two conditions will be considered; the emergence of one or more new sticky end(s) and the non-  
155 availability of sticky ends. The initial value of every node starts at 1.0. The DNA uptake rate is set at  
156 0.001 probability. Whenever a node is selected, the value of that node will be deducted by the DNA  
157 uptake rate. The formula for node concentration calculation is as follows:

158  $[Node_{NewCurrent}] = [Node_{Current}] - [Node_{UptakeRate}]$ .

159 The value of every node is evaluated during each cycle. The search will continue until the values of  
160 any node became nil (Table 1).

161

## 162 **2.5 DNA annealing**

163 Oligonucleotides were purchased from Integrated DNA Technologies Pte. Ltd. (USA). The  
164 complexes were formed by mixing stoichiometric quantities of DNA in an annealing buffer (40 mM  
165 Tris base, 2.5 mM EDTA, and 13 mM MgCl<sub>2</sub>) and annealing process from 90°C to 40°C for three  
166 hours using Eppendorf Mastercycler Pro S thermocycler (Eppendorf, Hamburg, Germany). To form  
167 the individual DNA shapes, four different oligonucleotides were mixed stoichiometrically in an  
168 annealing buffer and the final concentration was set to 0.5 μM.

169

## 170 **2.6 Gel electrophoresis**

171 The results of the annealing reactions were analyzed using non-denaturing gel electrophoresis  
172 containing 4% and 5% polyacrylamide gel (29:1 acrylamide:bisacrylamide), 0.75 mm thick and run at  
173 approximately 12V/cm-1 for 2 hours at 4°C. The running buffer contained 10 mM MgCl<sub>2</sub> and 1X TBE  
174 (89 mM Tris base, 89 mM Boric acid and 2 mM EDTA pH8.3) and the loading buffer contained 0.25%  
175 Bromophenol blue tracking dye and 30% glycerol. GelRed™ Nucleic Acid gel stain (Biotium, US)  
176 was used to stain the gel.

177

## 178 **2.7 Sample preparation and atomic force microscopy (AFM) imaging**

### 179 **2.7.1 Preparation of mica surface**

180 A 0.1% APTES ((3-aminopropyl) triethoxysilane) solution was prepared in ultrapure water. Then  
181 a drop (2 μL) of 0.1% APTES solution was deposited onto the freshly cleaved mica surface and the  
182 surface was rinsed with ultrapure water (20 μL) after 5 minutes incubation at room temperature.

183

## 184 **2.7.2 Sample preparation for AFM imaging**

185 The samples were diluted to 0.2 ng/ $\mu$ L with a buffer (40 mM Tris-HCl (pH 7.6), 13 mM MgCl<sub>2</sub>,  
186 2.5 mM EDTA). 2  $\mu$ L of the sample solution was placed onto the APTES-treated mica surface for 5  
187 minutes and the surface was later rinsed with the buffer (20  $\mu$ L) to remove unbound molecules.

188

## 189 **2.7.3 Atomic Force Microscopy (AFM) imaging**

190 The AFM images were collected using high-speed AFM (Nano Live Vision, Research Institute  
191 of Biomolecules Metrology Co., Tsukuba, Japan). The images were collected in tapping mode.

192

## 193 **3. Results**

### 194 **3.1 Formation of 3 x 4 DNA network using DNA polyominoes**

195 The size of the DNA network is fixed at 3 x 4 (i.e., 3 horizontal rows, and 4 vertical columns).  
196 Different configurations of heterogeneous shapes (monomino, tromino and tetrominoes) were  
197 generated to conform to the layout as illustrated in Fig. 4.

198

199 DNA sequences representing the respective shapes are generated using the autonomous protocol  
200 developed in our previous work (Ong et al., 2015). The program focuses on the stacking and merging  
201 of blocks to form DNA shapes. The program (Ong et al., 2015) relies on dependency information of all  
202 nucleotides positions with inter-binding linkage between different DNA strands (i.e., DNA-DNA  
203 binding). Details of the dependencies are available in the Supplementary Table S1-S5. The  
204 intermolecular bindings between various DNA shapes are "loosely" programmed using complementary  
205 sticky ends. The sticky ends are positioned at the intersection point, where different shapes are adjacent  
206 to each other. The default lengths of the sticky ends (for all DNA shapes) are set to 10 nucleotides. In  
207 order to further exploit the self-organisation ability of the molecule, the placement of matching sticky  
208 ends should be randomly placed. This will create an environment where optimisation between



209 competing shapes (i.e., survival of the most stable assembly) will help the stability of the desired  
210 structures as well as allowing total modularity to be enforced. However, in this study, the  
211 complementary sticky ends were predefined to ensure that different configurations of the 3 x 4 DNA  
212 network are attainable during wet-lab validation.

213

214 Molecular representation of our 3 x 4 DNA network showed that Set 1, 2, 3 and 4 have the same  
215 DNA shape compositions (i.e., the four heterogeneous DNA with different orientations). The size of  
216 set 1 is smaller as compared to set 2, 3, and 4. This is because set 1 only requires 25 nucleotides in  
217 each basic unit; the remaining sets require 40 nucleotides for their basic units. Set 5 has a different  
218 DNA shapes configuration. Compared to the existing techniques of DNA nanofabrication, our  
219 proposed approach increases the degree of freedom in designing the desired structure two-folds.  
220 Existing techniques focuses only on the sequence diversity of the design phase (i.e., sequences that  
221 conform to the scaffolds), while our approach introduces the combinatorics of the polyominoes shape  
222 into the equation thus allowing diversity not only in sequence, but also in the heterogeneous shapes  
223 composition (i.e., many sequences to many shapes configurations that conform to the desired  
224 structure).

225

### 226 **3.2 Gel electrophoresis and atomic force microscopy (AFM) imaging**

227 DNA sequences for each shape were added sequentially during the gel electrophoresis  
228 procedure (Fig. 5). AFM images of the structure were captured. Comparison with AFM images was  
229 conducted and the findings are encouraging. Successful clearly defined formations of DNAs that  
230 resemble the designed structures can be observed (Fig. 6).

231

232 All polyominoes shapes, with the exception of monomino, are single crossover DNA tiles or  
233 Holliday junctions. In contrast to the double-crossover (DX) motif which is structurally rigid (Li et al.,  
234 1996), the structure of the Holliday junction motif is inherently floppy (Rothemund, 2005). This is

235 because the four-way junction of the motif alternates between one of two different “stacked-X”  
236 conformations (Duckett et al., 1988; Murchie et al., 1989), thus forming an approximately 60° angle  
237 (Mao et al., 1999) between the two DNA helices. Given this natural profile, the final structure captured  
238 using the AFM is floppy as the self-assembly of multiple Holliday junctions has an approximately 60°  
239 native between the two DNA helices as observed in the figure.

240

#### 241 **4. Discussion**

242 To address the complexity of determining the "many sequences to many shapes configurations"  
243 allowances introduced in our approach, we have annotated the base pairing probability using the  
244 concept of undirected graphs (i.e., each node/vertex can be visited more than once; with no emphasis  
245 on the order of the path taken. In our implementation, “nodes” represent DNA segments while the  
246 “edges” represent binding affinity between nodes. The decision of traversing any of these nodes are  
247 dependent on the free sticky ends resulted from prior binding (edge) (Fig. 7). As long as the new  
248 sticky ends have a probability value of more than the defined threshold value (0.7), it is predicted to be  
249 able to bind to the existing parent DNA (node). This process will be repeated iteratively for each node  
250 (similar to a greedy search where all paths are traversed).

251

252

253 Therefore, the number of graphs is equivalent to the number of potential structures that can be  
254 generated from a set of DNA strands. This number includes both the desired and misfolded structures.  
255 For example, the shapes configuration of set 5 produces 31 different graphs with only 21 graphs  
256 indicating the formation of the desired structure. Thus, there are 10 misleading paths that are biased  
257 towards unfavourable folding leading to the formation of mismatch structures. The number of  
258 occurrences for binding affinity close to 1.0 indicates the level of competition between the unintended  
259 nodes (i.e., not design to form base pair). Thus, the number of competitions is linear to the number of  
260 graphs that will be generated. Our search revealed that set 4 has the highest number of graphs

261 generated, followed by set 3, 2, 1 and 5 respectively (Table 2). This contributed to the higher number  
262 of binding affinities with values near to 1.0.

263

264 The value  $P_{i,j}$  represents the relative binding affinity between each DNA segment estimated using  
265 the thermodynamics free energy from the program Duplexfold (Reuter and Mathews, 2010).  $P_{i,j}$  has  
266 the value of 1.0, if the intended binding between nodes is a perfect complementary pair. In our  
267 calculation, partially complement ( $P_{i,j} < 1.0$ ) of DNA segments is still considered. However, these  
268 partially complements segments have the tendency to create false routes (causing the emergence of  
269 sticky ends) and eventually resulted in the formation of false structures or miscellaneous aggregates.  
270 The correct graphs are representations of all the nodes visited exactly once and the edges taken by each  
271 node are correctly linked as designed, regardless of the starting points. The order of the completed  
272 routes will provide a blueprint for the DNA sequences to form the desired structures.

273

#### 274 **Acknowledgements**

275 We gratefully acknowledge Professor Hiroshi Sugiyama from the Department of Chemistry, Graduate  
276 School of Science, Kyoto University and Institute for Integrated Cell-Material Sciences (WPI-iCeMS),  
277 Kyoto University and Dr. Yuki Suzuki from the Department of Chemistry, Graduate School of  
278 Science, Kyoto University for their assistance and expertise in AFM imaging. Acknowledgement is  
279 extended to both Dr. Zamri Radzi and Ms. Nabila Farhana from the Department of Paediatric Dentistry  
280 & Orthodontics, Faculty of Dentistry, University of Malaya in providing AFM imaging for the study.  
281 This research is supported by the High Impact Research Grant UM.C/625/1/HIR/MoE/FCSIT/002 (H-  
282 22001-00-B0002) from the Ministry of Higher Education, Malaysia and University of Malaya.

283

#### 284 **Author contributions statement**

285 Conceived and designed the experiments: HSO MSR MFR EIR. Performed the experiments: HSO  
286 MSR. Analyzed the data: HSO MSR MFR EIR. Contributed reagents/materials/analysis tools: HSO

287 MSR NHAK MFR EIR. Wrote the paper: HSO MSR NHAK MFR EIR.

288

289 **Additional information.**

290 **Competing financial interests.** The authors declare no competing financial interests.

291 **References**

- 292 Alves, C., Iacovelli, F., Falconi, M., Cardamone, F., Morozzo Della Rocca, B., de Oliveira, C.L., Desideri, A.,  
293 (2016) A Simple and Fast Semiautomatic Procedure for the Atomistic Modeling of Complex DNA  
294 Polyhedra. *J Chem Inf Model.* 56, 941-949.
- 295 Amir, Y., Ben-Ishay, E., Levner, D., Ittah, S., Abu-Horowitz, A., Bachelet, I., (2014) Universal computing by  
296 DNA origami robots in a living animal. *Nature Nanotechnology* 9, 353-357.
- 297 Benenson, Y., Gil, B., Ben-Dor, U., Adar, R., Shapiro, E., (2004) An autonomous molecular computer for  
298 logical control of gene expression. *Nature* 429, 423.
- 299 Biggs, N.L., Lloyd, E.K., Wilson, R.J., (1986) *Graph Theory 1736-1936.* Oxford University Press, New York.
- 300 Birac, J.J., Sherman, W.B., Kopatsch, J., Constantinou, P.E., Seeman, N.C., (2006) Architecture with GIDEON,  
301 A Program for Design in Structural DNA Nanotechnology. *J Mol Graph Model* 25, 470-480.
- 302 Ding, B., Seeman, N.C., (2006) Operation of a DNA robot arm inserted into a 2D DNA crystalline substrate.  
303 *Science* 314, 1583.
- 304 Douglas, S.M., Bachelet, I., Church, G.M., (2012) A logic-gated nanorobot for targeted transport of  
305 molecular payloads. *Science* 335, 831.
- 306 Douglas, S.M., Marblestone, A.H., Teerapittayanon, S., Vazquez, A., Church, G.M., Shih, W.M., (2009) Rapid  
307 prototyping of 3D DNA-origami shapes with caDNAno. *Nucleic Acids Res* 37, 5001-5006.
- 308 Duckett, D.R., Murchie, A.I.H., Diekmann, S., Kitzing, E.V., Kemper, B., Lilley, D.M.J., (1988) The structure of  
309 the Holliday junction, and its resolution. *Cell* 55, 79-89.
- 310 Han, D., Pal, S., Nangreave, J., Deng, Z., Liu, Y., Yan, H., (2011) DNA origami with complex curvatures in  
311 three-dimensional space. *Science* 332, 342-346.
- 312 Ke, Y., Ong, L.L., Shih, W.M., Yin, P., (2012) Three-Dimensional Structures Self-Assembled from DNA  
313 Bricks. *Science* 338, 1177-1183
- 314 Kuzuya, A., Komiyama, M., (2010) DNA origami: Fold, stick, and beyond. *Nanoscale. Review.* 2, 310-322.
- 315 Li, X., Yang, X., Qi, J., Seeman, N.C., (1996) Antiparallel DNA Double Crossover Molecules As Components  
316 for Nanoconstruction. *J. Am. Chem. Soc.* 118, 6131-6140.
- 317 Mao, C., LaBean, T.H., Reif, J.H., Seeman, N.C., (2000) Logical computation using algorithmic self-assembly  
318 of DNA triple-crossover molecules. *Nature* 407, 493-496.
- 319 Mao, C., Sun, W., Seeman, N.C., (1999) Designed Two-Dimensional DNA Holliday Junction Arrays  
320 Visualized by Atomic Force Microscopy. *American Chemical Society* 121, 5437-5443.
- 321 Marchi, A.N., Saaem, I., Vogen, B.N., Brown, S., LaBean, T.H., (2014) Toward Larger DNA Origami. *Nano*  
322 *Letter* 14, 5740-5747.
- 323 Markham, N.R., Zuker, M., (2008) UNAFold: software for nucleic acid folding and hybridization. *Methods*  
324 *Molecular Biology* 453, 3-31.
- 325 Murchie, A.I.H., Clegg, R.M., Kitzing, E.V., Duckett, D.R., Diekmann, S., Lilley, D.M.J., (1989) Fluorescence  
326 energy transfer shows that the four-way DNA junction is a right-handed cross of antiparallel molecules.  
327 *Nature* 341, 763-766.
- 328 Ong, H.S., Rahim, M.S., Firdaus-Raih, M., Ramlan, E.I., (2015) DNA Tetrominoes: The Construction of DNA  
329 Nanostructures Using Self-Organised Heterogeneous Deoxyribonucleic Acids Shapes. *PLoS ONE* 10,  
330 e0134520.
- 331 Pinheiro, A.V., Han, D., Shih, W.M., Yan, H., (2011) Challenges and opportunities for structural DNA  
332 nanotechnology. *Nature Nanotechnology* 6, 763-772.
- 333 Ramlan, E.I., Zauner, K.-P., (2013) In-silico design of computational nucleic acids for molecular  
334 information processing. *Journal of Cheminformatics* 5, 22.
- 335 Reuter, J.S., Mathews, D.H., (2010) RNAstructure: software for RNA secondary structure prediction and  
336 analysis. *BMC Bioinformatics* 11, 129.

337 Rothemund, P.W.K., (2005) DNA self-assembly with floppy motifs – single crossover lattices. *Foundations*  
338 *of Nanoscience, Self-Assembled Architectures and Devices, Proceedings of FNANO'05*. J.H. Reif eds, pp.  
339 185–186.  
340 Rothemund, P.W.K., (2006) Folding DNA to create nanoscale shapes and patterns. *Nature* 440, 297–302.  
341 Rothemund, P.W.K., Papadakis, N., Winfree, E., (2004) Algorithmic self-assembly of DNA Sierpinski  
342 triangles. *PLoS Biol.* 2, e424.  
343 Seeman, N.C., (1982) Nucleic-acid junctions and lattices. *J Theor Biol* 99, 237–247.  
344 Wei, B., Dai, M., Yin, P., (2012) Complex shapes self-assembled from single-stranded DNA tiles. *Nature*  
345 485, 623-626.  
346 Williams, S., Lund, K., Lin, C., Wonka, P., Lindsay, S., Yan, H., (2008) Tiamat: a three-dimensional editing  
347 tool for complex DNA structures. In: Goel, A., Simmel, F.C., Sosík, P. (Eds.), *The 14th International Meeting*  
348 *on DNA Computing Proceedings, Czech Republic: Silesian University in Opava*, pp. 112–121.  
349 Winfree, E., (1996) On the computational power of DNA annealing and ligation. In: Lipton, R.J., Baum, E.B.  
350 (Eds.), *DNA-based computers*. American Mathematical Society, Providence, Rhode Island, pp. 199–221.  
351 Winfree, E., (1998) Algorithmic self-assembly of DNA. California Institute of Technology.  
352 Yin, P., Hariadi, R.F., Sahu, S., Choi, H.M.T., Park, S.H., LaBean, T.H., Reif, J.H., (2008) Programming DNA  
353 Tube Circumferences. *Science* 321, 824-826.  
354 Zauner KP. (2005). From Prescriptive Programming of Solid-State Devices to Orchestrated Self-  
355 organisation of Informed Matter. *Unconventional Programming Paradigms*. 2005;3566:47-55.  
356 Zhu, J., Wei, B., Yuan, Y., Mi, Y., (2009) UNIQUIMER 3D, a software system for structural DNA  
357 nanotechnology design, analysis and evaluation. *Nucleic Acids Research* 37, 2164-2175.

358

359

360

361

362

363

364

365

366

367

368

369

370

371

372

373

374

375

376

377 **Figure Legend**

378

379 **Fig. 1.** Self-organisation of DNA polyominoes. (A) The formation of DNA polyominoes shapes using  
380 a single or multiple basic blocks. Each block may or may not have connector(s) to form inter-assembly  
381 between multiple polyominoes shapes. (B) The conceptual illustration of the assembly for a desired  
382 DNA configuration. The polyominoes shapes are assembled using complementary connectors (case 1).  
383 The assembly of polyominoes shapes would not occur without the presence of the connector motifs  
384 (case 2) or when non-complementary connector exists (case 3). DNA strands are used to assemble each  
385 individual polyominoes shape. Different DNA strands are labelled as DNA 1, DNA 2, DNA 3 and  
386 DNA 4. Whenever there is a presence of a connector, its corresponding region (in another DNA  
387 sequence) will have sticky end to enable two polyominoes shapes to bind together. The assembly of  
388 four DNA strands used to form polyominoes shapes will twist the double-stacked DNA strands at an  
389 approximately 60° angle (Mao et al., 1999), which results in the DNA polyominoes shape to be floppy.

390

391 **Fig. 2.** Conceptual representation of the formation of DNA polyominoes shapes. (A-H) represents the  
392 formation of T-shape, W-shape, F-shape, E-shape, V-shape, L-shape, B-shape and I-shape. The  
393 resulted four-way junction in the DNA polyominoes shapes (except for I-shape) are structurally floppy.  
394 Basic blocks were used to form four long continuous single-stranded DNAs (ssDNAs). DNA strands  
395 were represented as DNA 1, DNA 2, DNA 3 and DNA 4. The arrows in the DNA strands indicated the  
396 5' to 3' direction.

397

398 **Fig. 3.** An example segmentation for DNA heterogeneous shapes (A) DNA duplex (I-Shape) and (B)  
399 Holliday Junctions (B, E, W, I, T, F, L, V-shape).

400

401 **Fig. 4.** The nucleotides arrangements of the 3 x 4 DNA network for (A) Set 1 (B) Set 2 (C) Set 3 (D)  
402 Set 4 and (E) Set 5. The arrows represent 5' to 3' terminal and the dotted lines represent  
403 complementary binding. The symbol (\*) on the 3 x 4 DNA network (right) represents the location of  
404 the sticky ends used for intermolecular binding between different DNA shapes.

405

406 **Fig. 5.** Gel electrophoresis result for (A) Set 1 on 8% non-denaturing gel (B) Set 2 on 5% non-  
407 denaturing gel (C) Set 3 on 5% non-denaturing gel (D) Set 4 on 4% non-denaturing gel and (E) Set 5  
408 on 5% non-denaturing gel.

409

410 **Fig. 6.** AFM images showed the image size of (A) Set 1 (B) Set 2 (C) Set 3 (D) Set 4 and (E) Set 5 at  
411 100 nm x 75 nm. Each region of the image is labelled with orange color and the AFM images are  
412 compared with the predicted representation (Design of 3 x 4 DNA network). The final structures  
413 captured in the AFM images are structurally floppy due to the single crossover lattices in each DNA  
414 polyominoes shape (except I-shape) that has a native angle of approximately 60°.

415

416 **Fig. 7.** The connectivity map for each node in (A) Set 1 (B) Set 2 (C) Set 3 (D) Set 4 and (E) Set 5.  
417 Black lines indicate the binding affinity between the respective nodes, which is equals to 1.0. Blue  
418 dashed lines indicate nodes that are derived from the same DNA strands, which are then used to decide  
419 on the emergence of potential sticky ends binding region. Orange lines reveal the nodes with the

420 binding affinity value of  $0.7 < P_{ij} < 1.0$ . The colour legends represent the type of DNA shapes  
 421 involved in the configuration of the network.

422

423 **Tables**

424

425 **Table 1.** Algorithm for computing all probable paths.

---

```

1: Split DNA into different segments (Node), N
2: Define bounded node (form base pairing)=Nb
3: Define unbound node (free sticky ends)=Nu,
4: Initialise all initial node concentration, [N] = 1.0
5:   For each Nu do
6:     Check probability matrix
7:     If Pe > ThresholdValue, 0.7
8:       Record new node, NTempoNew bind to Nb
9:       For each NTempoNew do
10:        Check all nodes concentration, [N] in the solution
11:        If [Nall] > 0% then
12:          NTempoNew is bind to Nu
13:          Compute new Sticky Ends, Nu
14:          Record Nu
15:          Update latest total solution concentration
16:          [NLatest] = [NCurrent] - [NUptakeRate]
17:        else
18:          No binding, [NNewCurrent] = [NNewCurrent]
19:        end for
20:      end if
21:    end for

```

---

426

427

428 **Table 2:** Summary of the numbers of graphs generated through the searches.

Combinations	Number of correct graphs	Number of graphs	Binding affinity $0.7 < P_{ij} < 1.0$
Set 1	17	200	0.74, 0.76
Set 2	16	469	0.71, 0.72, 0.75, 0.77
Set 3	16	605	0.72, 0.72, 0.72, 0.73, 0.75
Set 4	12	757	0.72, 0.72, 0.72, 0.73, 0.77, 0.79, 0.84
Set 5	21	31	0.73

---

429

430

431

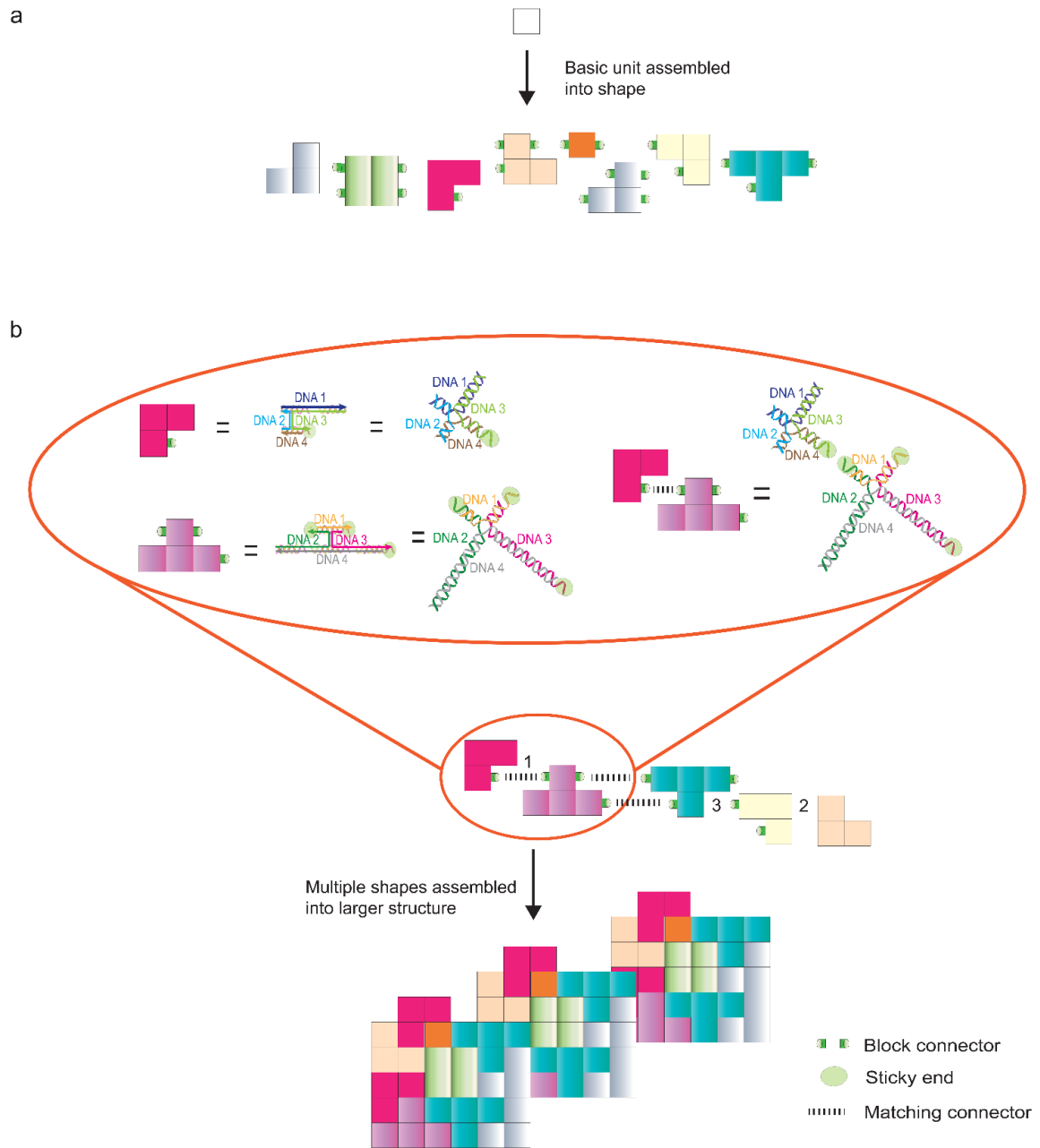


Figure 1

432

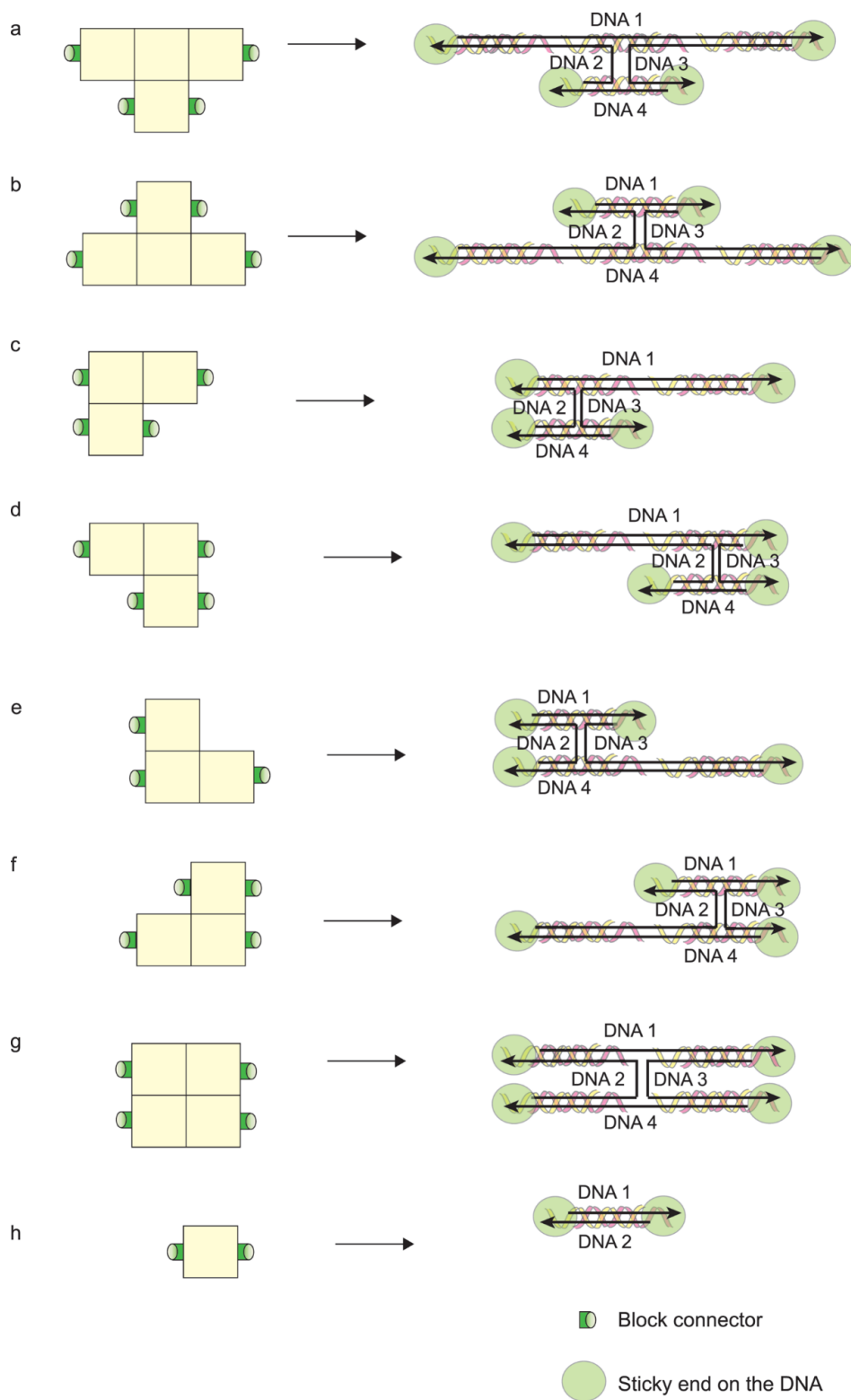
433

434

435

436





437  
 438  
 439  
 440

**Figure 2**

441

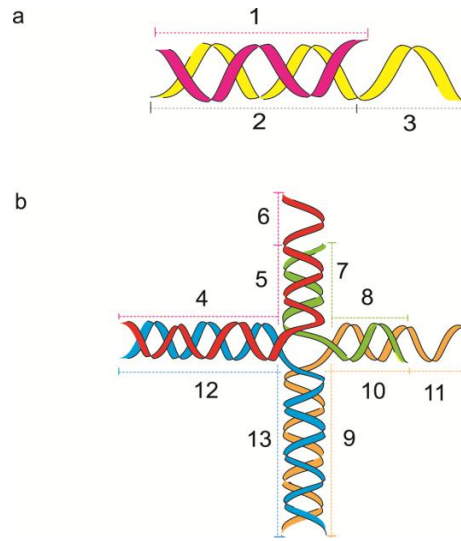


Figure 3

442

443

444

445

446

447

448

449

450

451

452

453

454

455

456

457

458

459

460

461

462

463

464

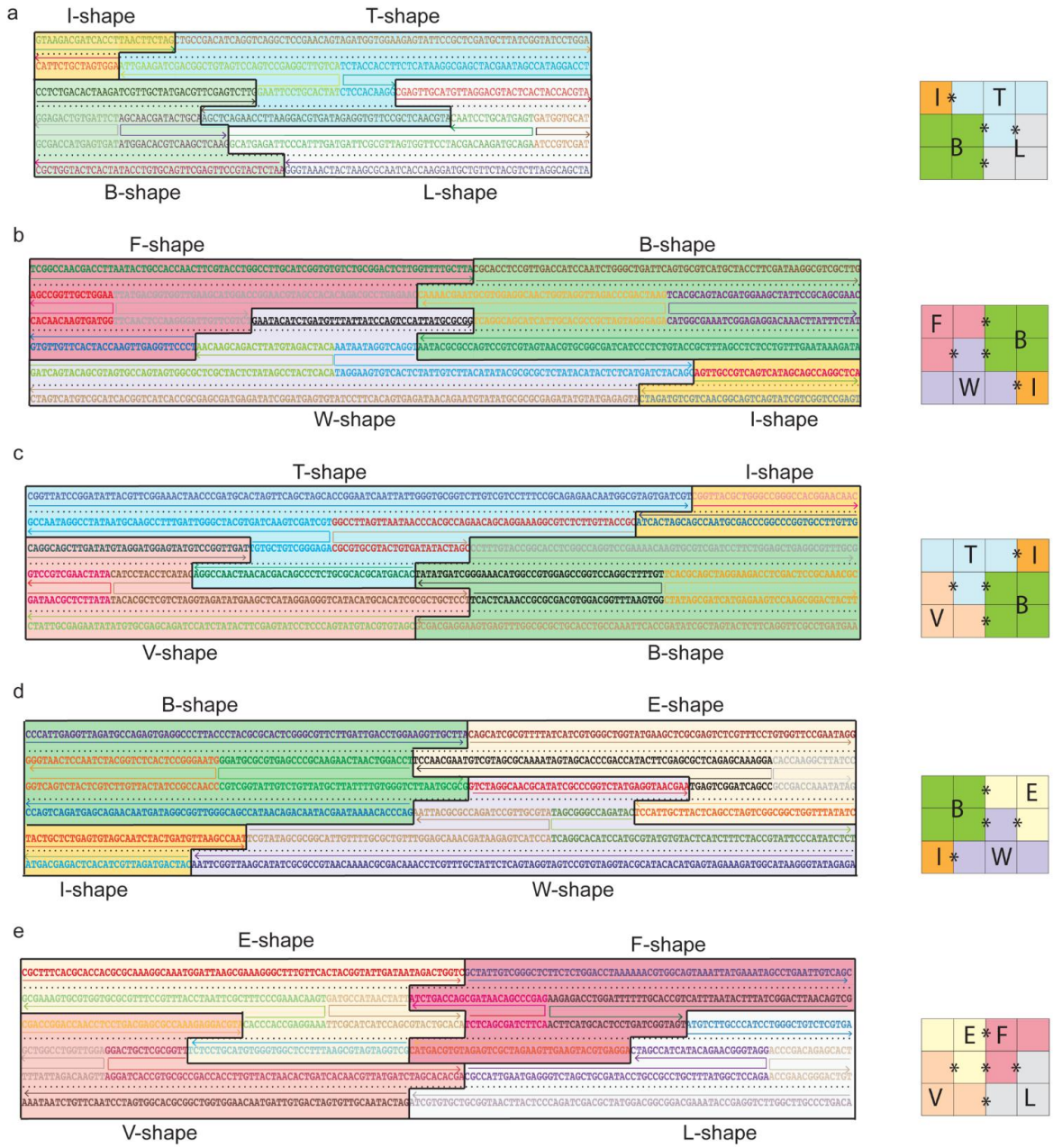
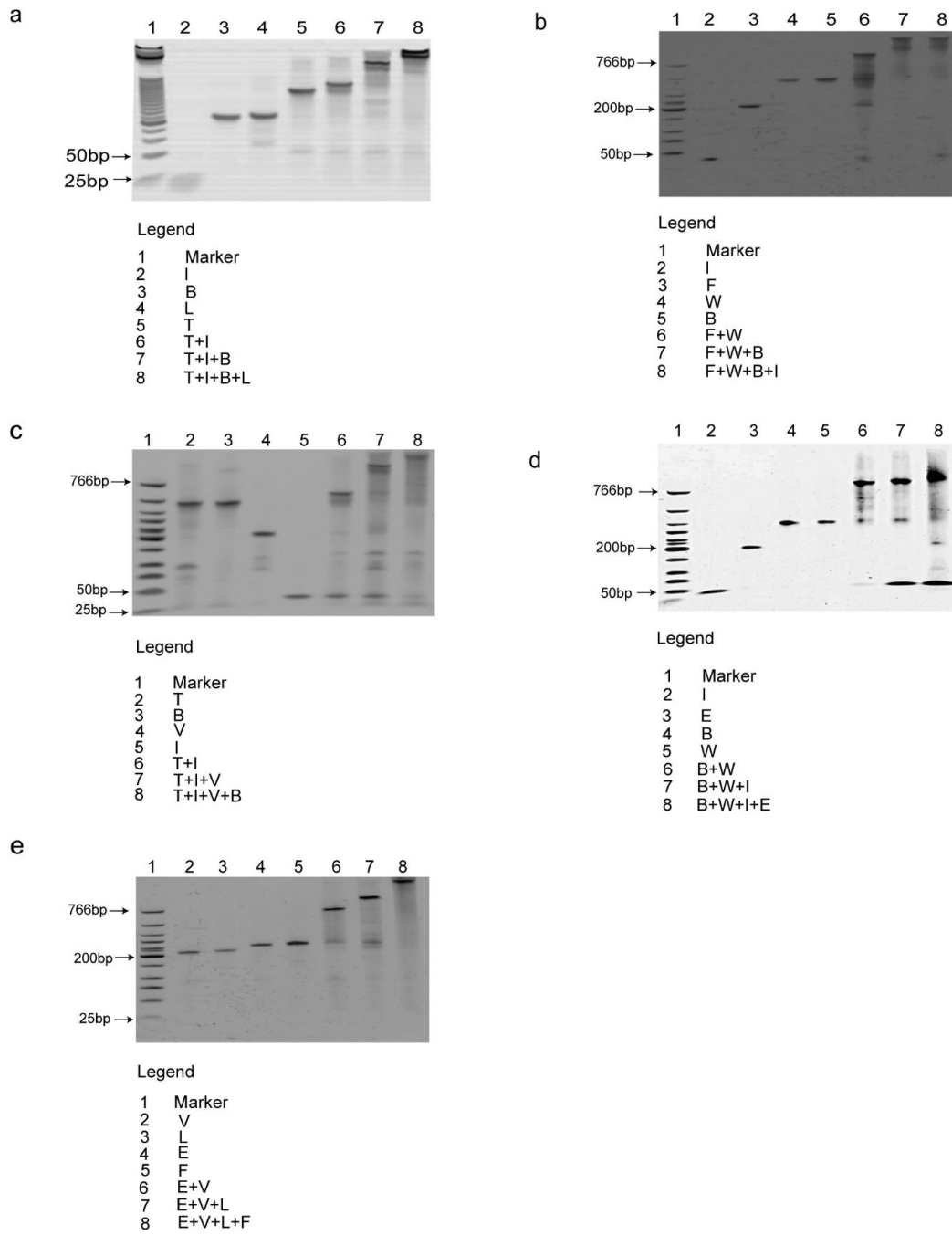


**Figure 4**

465  
466  
467  
468  
469  
470  
471  
472  
473

474

475



476

477

478

479

480

Figure 5

AFM images (100 nm X 75 nm)

Design of 3x4 DNA network

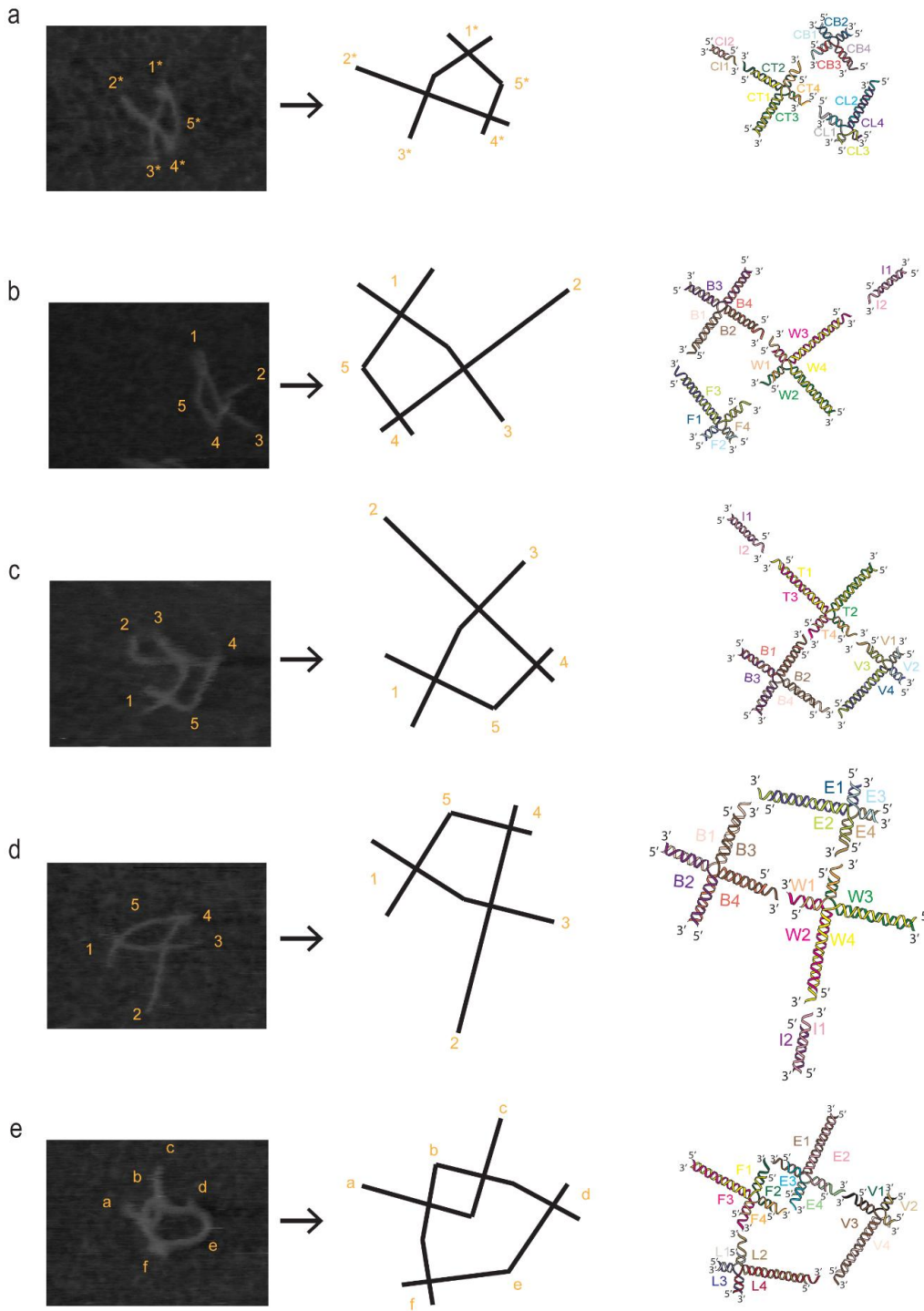


Figure 6

481

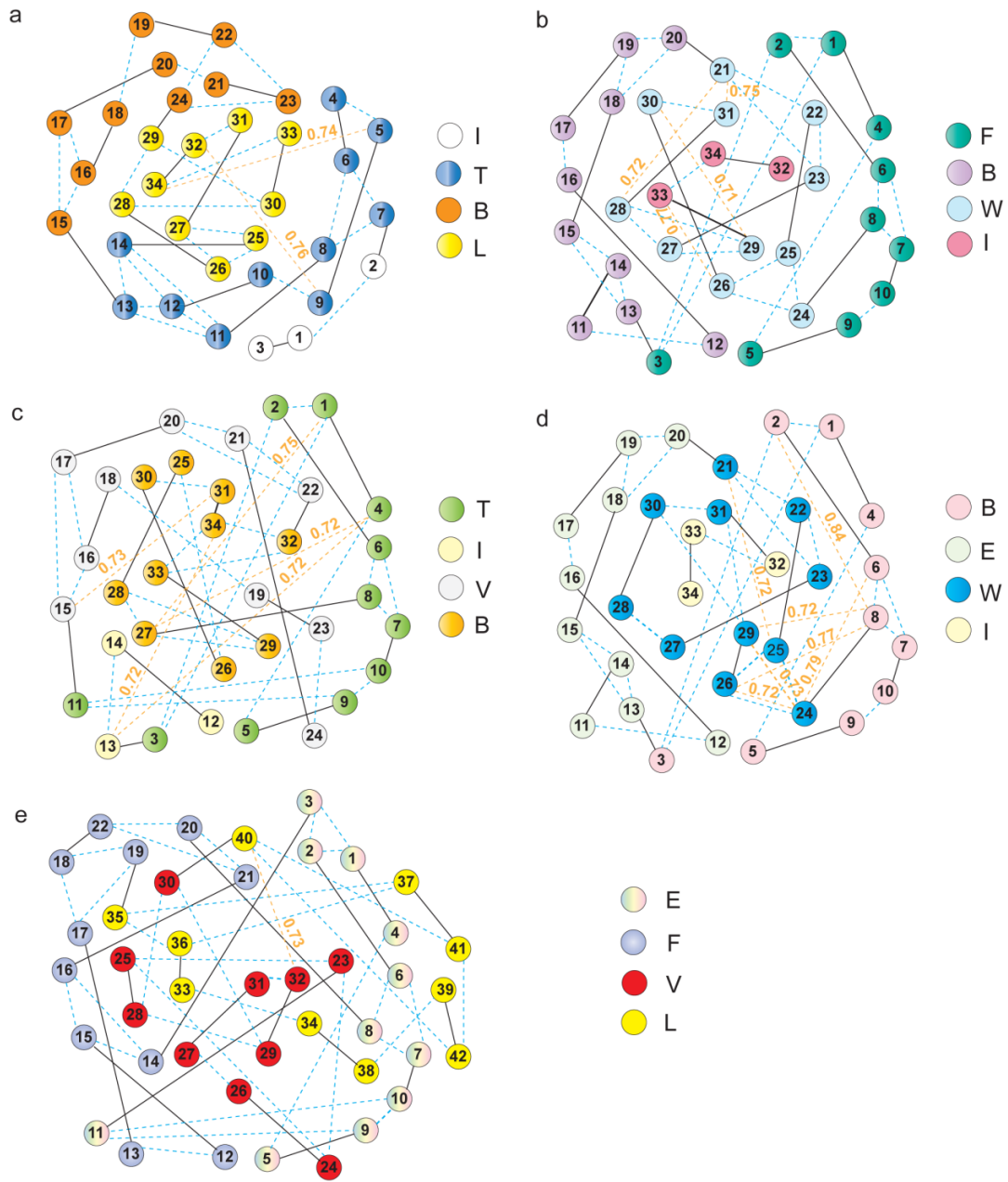
482

483

484

485

486



487

488

489

490

491

Figure 7

Figure 1 R  
[Click here to download high resolution image](#)

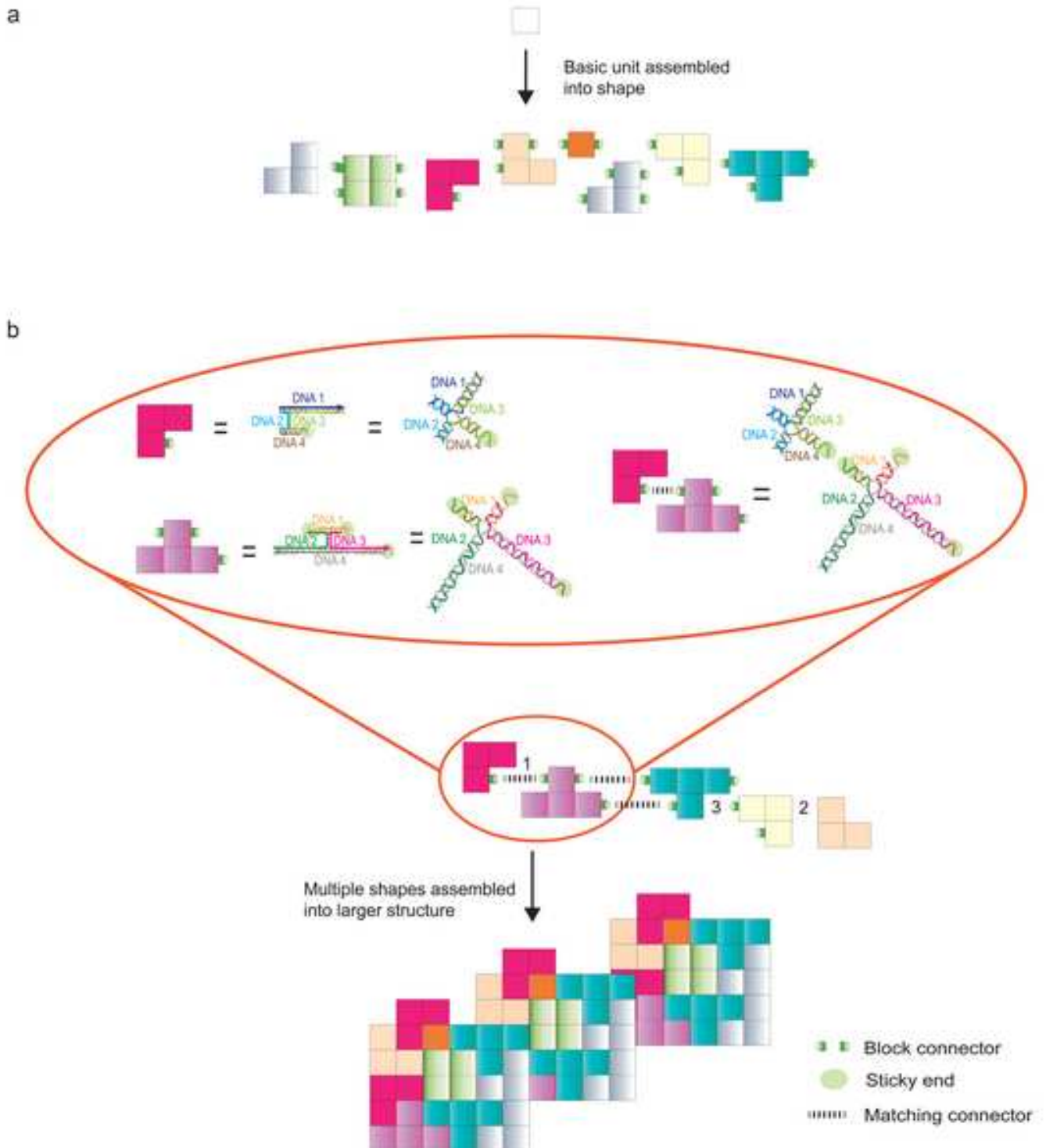


Figure 2 R

[Click here to download high resolution image](#)

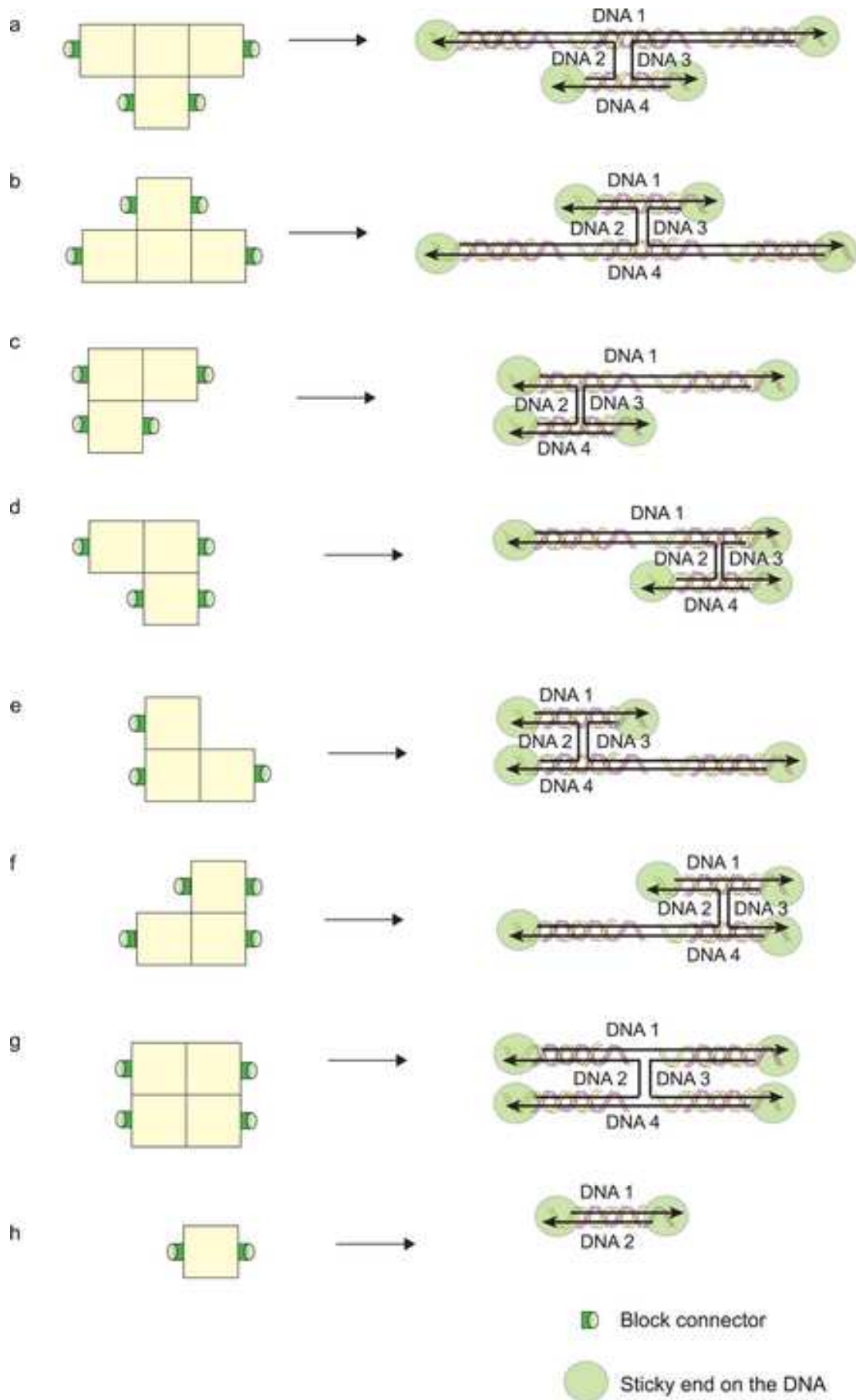




Figure 3 R  
[Click here to download high resolution image](#)

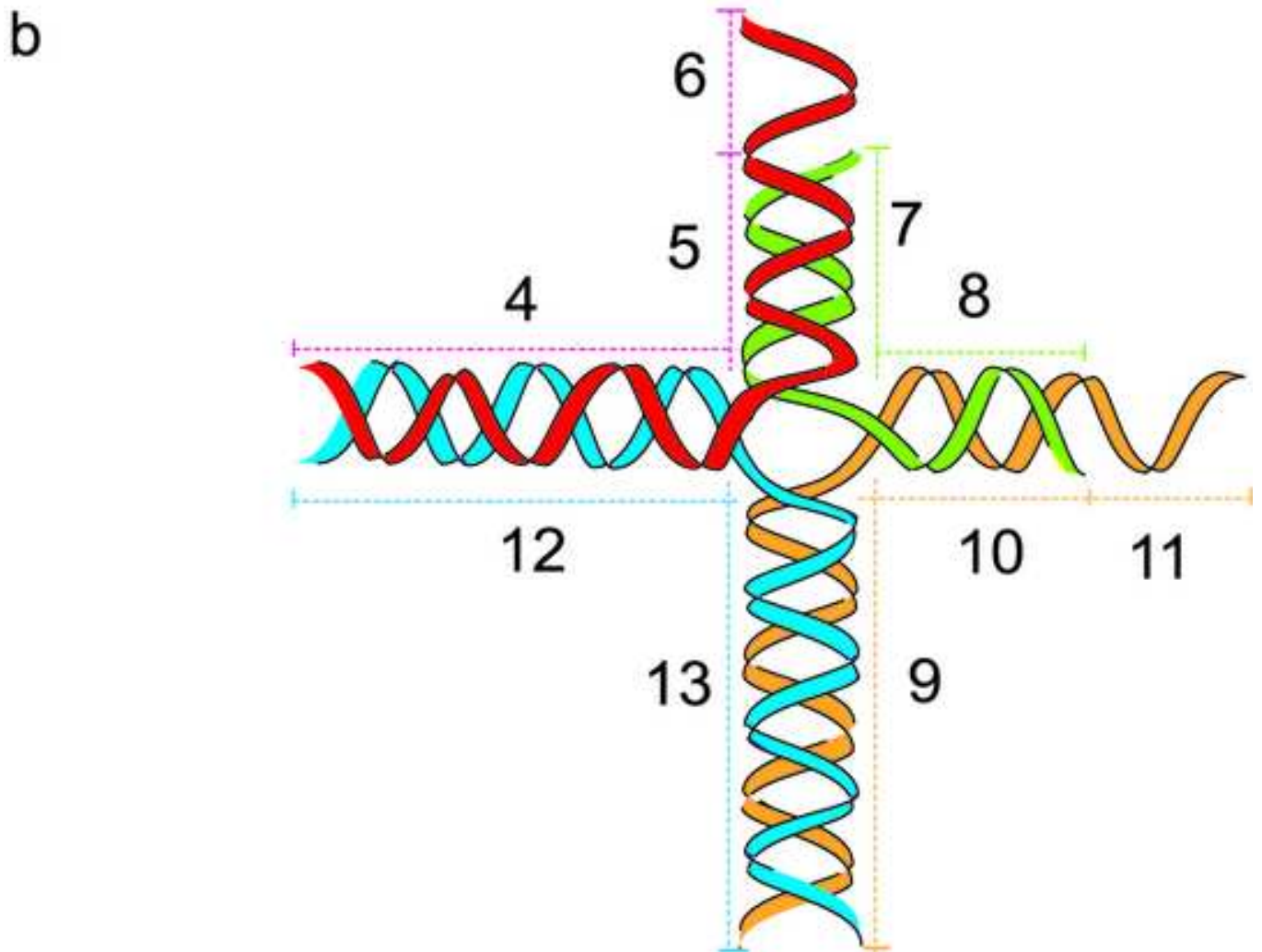
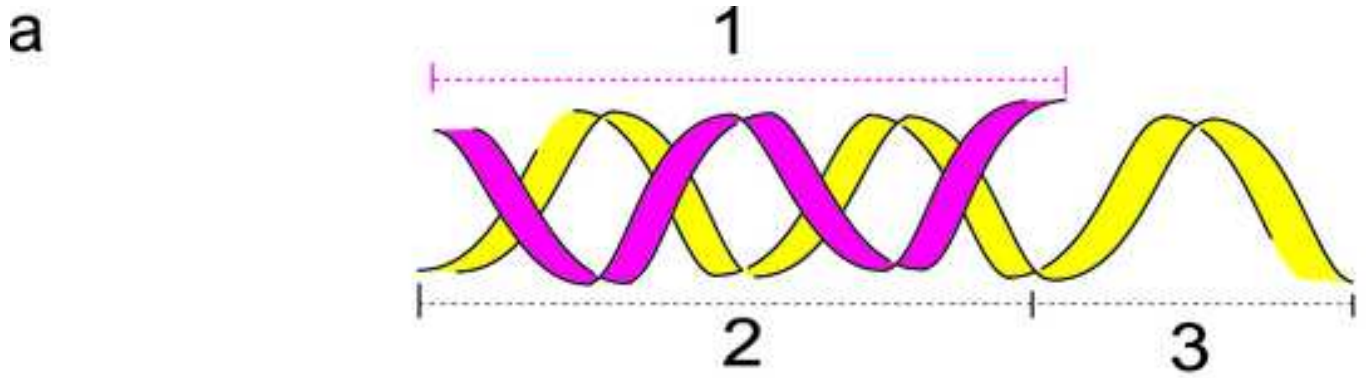


Figure 4 R  
[Click here to download high resolution image](#)

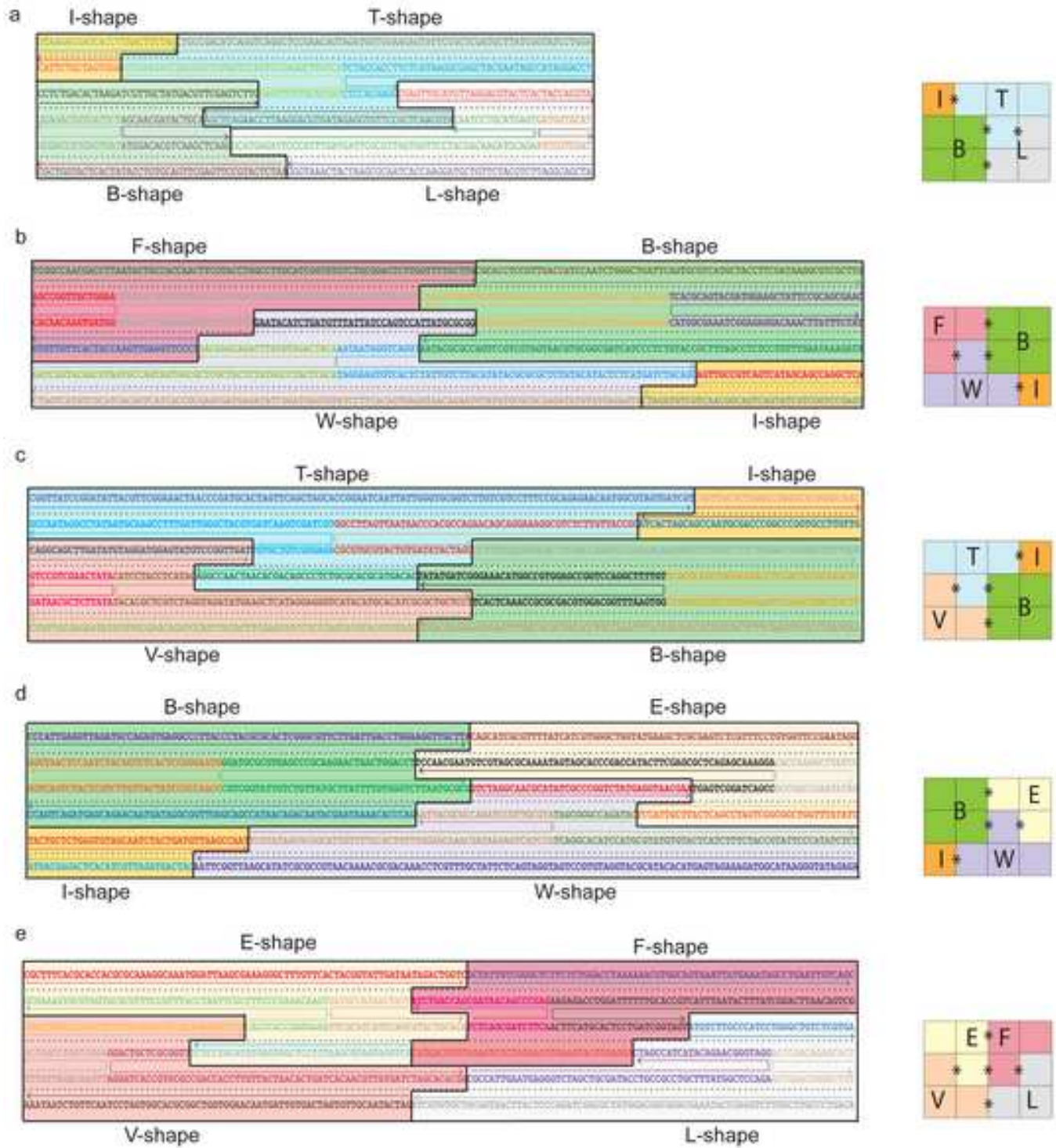
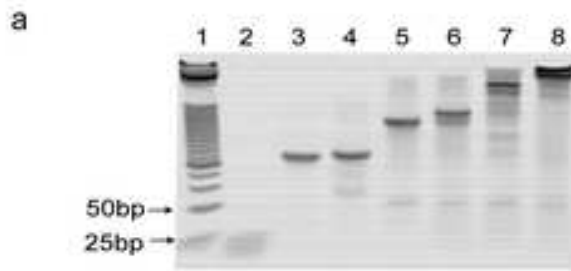


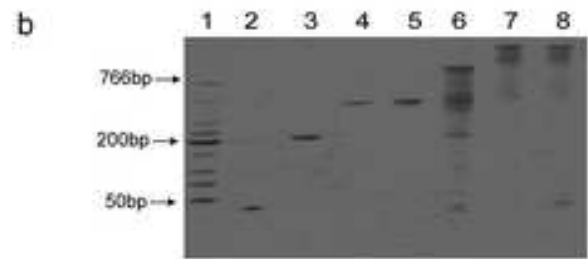
Figure 5 R

[Click here to download high resolution image](#)



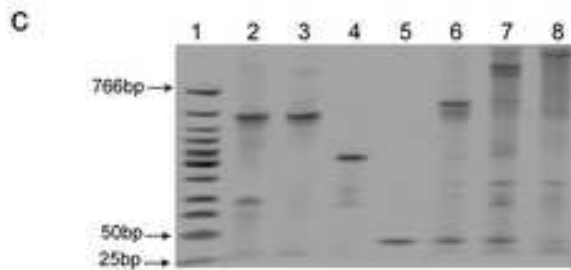
Legend

- |   |         |
|---|---------|
| 1 | Marker  |
| 2 | I       |
| 3 | B       |
| 4 | L       |
| 5 | T       |
| 6 | T+I     |
| 7 | T+I+B   |
| 8 | T+I+B+L |



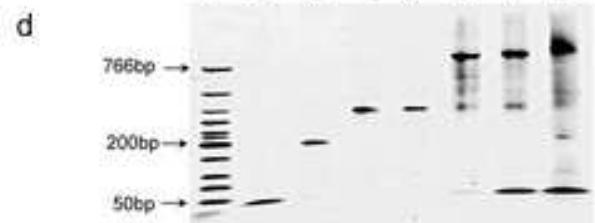
Legend

- |   |         |
|---|---------|
| 1 | Marker  |
| 2 | I       |
| 3 | F       |
| 4 | W       |
| 5 | B       |
| 6 | F+W     |
| 7 | F+W+B   |
| 8 | F+W+B+I |



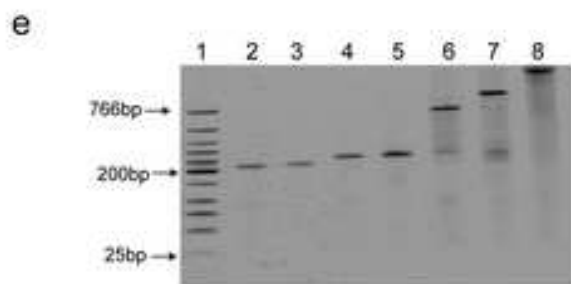
Legend

- |   |         |
|---|---------|
| 1 | Marker  |
| 2 | T       |
| 3 | B       |
| 4 | V       |
| 5 | I       |
| 6 | T+I     |
| 7 | T+I+V   |
| 8 | T+I+V+B |



Legend

- |   |         |
|---|---------|
| 1 | Marker  |
| 2 | I       |
| 3 | E       |
| 4 | B       |
| 5 | W       |
| 6 | B+W     |
| 7 | B+W+I   |
| 8 | B+W+I+E |



Legend

- |   |         |
|---|---------|
| 1 | Marker  |
| 2 | V       |
| 3 | L       |
| 4 | E       |
| 5 | F       |
| 6 | E+V     |
| 7 | E+V+L   |
| 8 | E+V+L+F |

Figure 6 R

[Click here to download high resolution image](#)

AFM images (100 nm X 75 nm)

Design of 3x4 DNA network

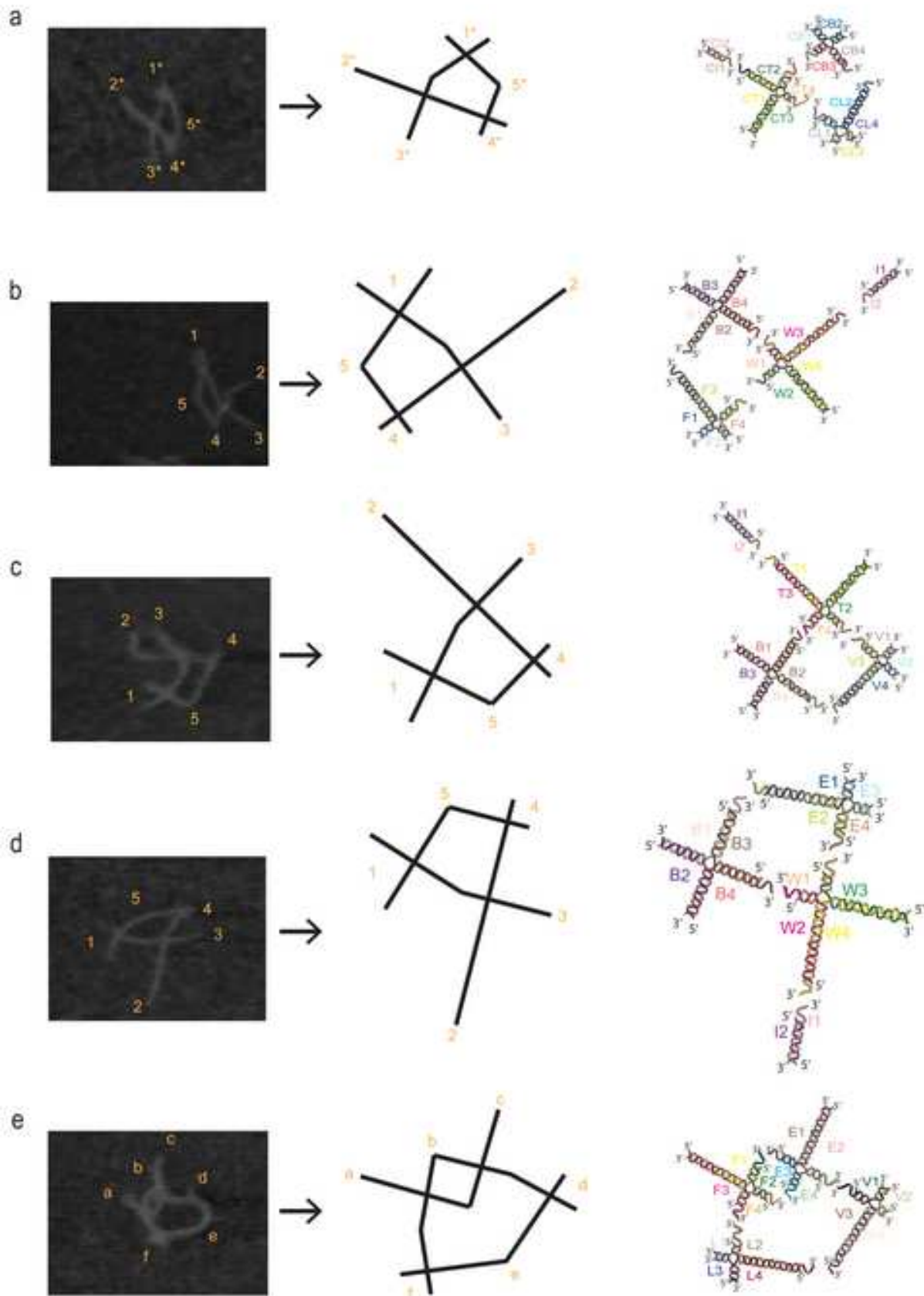
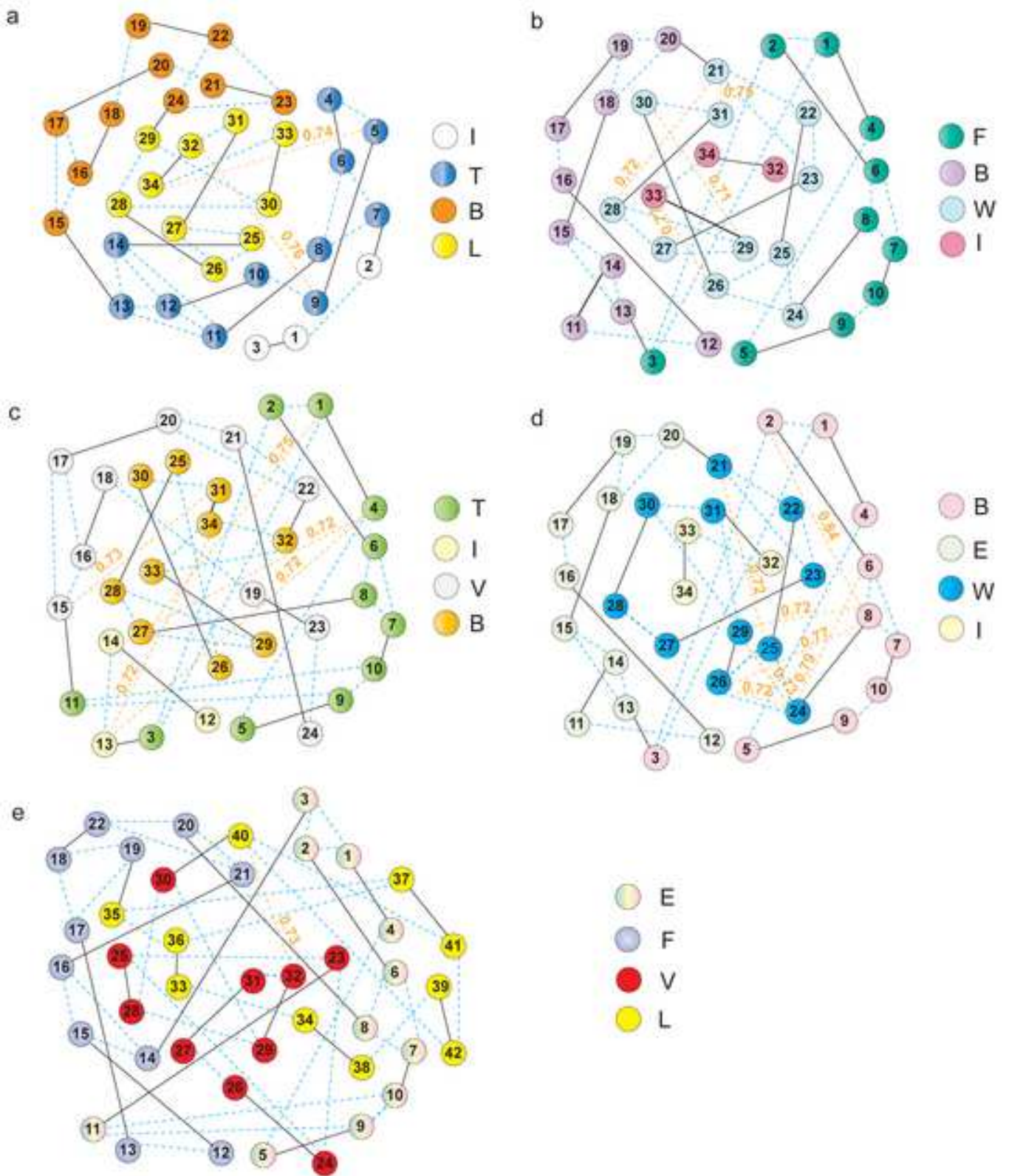


Figure 7 R  
[Click here to download high resolution image](#)



**Supplementary File R**

[Click here to download Supplementary File: Supporting Information.doc](#)